Copy No. _____

Defence Research and Development Canada
Recherche et développement pour la défense Canada

DEFENCE R&D DÉFENSE

Measurement and Analysis of Sound Speed Dispersion During SAX04

Final Report for Office of Naval Research Award N000140310883

John C. Osler
Paul C. Hines

Prepared for:
US Office of Naval Research
875 North Randolph Street, Suite 1425, Code 321OA
Arlington, VA 22203-1995, USA

Defence R&D Canada – Atlantic

External Client Report
DRDC Atlantic ECR 2010-338
December 2010

Canada

This page intentionally left blank.

Measurement and Analysis of Sound Speed Dispersion During SAX04

Final Report for Office of Naval Research Award N000140310883

John C. Osler
Paul C. Hines

Prepared for:
US Office of Naval Research
875 N Randolph Street, Suite 1425, Code 321OA,
Arlington, VA 22203-1995, USA

Defence R&D Canada – Atlantic

External Client Report
DRDC Atlantic ECR 2010-338
December 2010

Principal Author

Original signed by John Osler

John Osler

Approved by

Original signed by Dan Hutt

Dan Hutt

Head / Underwater Sensing

Approved for release by

Original signed by Calvin Hyatt

Calvin Hyatt

Chief Scientist

Abstract

Sharing the same experimental apparatus, two complementary techniques were developed to measure the frequency-dependent speed of sound in marine sediments during the SAX04 sea-trial. The first technique enabled direct time-of-flight measurements of acoustic wave speed along all three Cartesian axes. The second technique determined the acoustic wave speed based on the arrival angle of pulses generated in the water column and refracted upon entry into the seabed. None of the results could be modeled or explained when the seabed was parameterized as a sand half-space. However, both techniques suggested the presence of a thin muddy layer, 0.05–0.2 m thick within the top 1 m of the sediment. For the arrival angle technique, the layer explains the complicated frequency- and geometry-dependent results; unfortunately, the interference from the layer dominated the arrival angle behavior to the extent that sound speed dispersion could not be determined unambiguously. For the time-of-flight technique, the acoustic wave speed was found to be dispersive in the frequency regime from 0.6 to 20 kHz with the normalized wave speed increasing from approximately 1.05 to 1.13. However, the layer caused the measured sound speeds to be lower than what a simplified poro-elastic model would predict, unless one accounts for the higher porosity material present within the buried layer.

This page intentionally left blank.

Executive summary

Measurement and Analysis of Sound Speed Dispersion During SAX04: Final Report for Office of Naval Research Award N000140310883

John C. Osler: Paul C. Hines; DRDC Atlantic ECR 2010-338; Defence R&D Canada – Atlantic; December 2010.

Introduction: Sediment sound-speed measurements during SAX99, a U.S. Office of Naval Research Departmental Research Initiative with a field experiment in 1999 in the Gulf of Mexico, suggested that the speed of sound traveling through marine sediments depends on the frequency of the sound (i.e., sound speed dispersion), particularly when the seabed is principally composed of sand. Sound-speed dispersion measurements are being used as a fundamental metric for evaluating competing theories, some new and some revived, for sound propagation in marine sediments. Historically, it has been difficult to make sound-speed measurements below 10 kHz. As a result, there is a paucity of experimental results and they tend to have large uncertainties, or they are relative rather than absolute values. Measurements in the 1–10 kHz frequency band are critical as this is where the most pronounced sound-speed dispersion was observed during SAX99, and where the most significant differences in the theories are predicted to occur. To address these issues, DRDC developed two experimental techniques that share the same experimental apparatus, to measure sound-speed dispersion from approximately 0.6 to 20 kHz during SAX04.

Results: The first technique is a direct time-of-flight measurement of acoustic wave speed along all three Cartesian axes, the second determines acoustic wave speed based on the arrival angle of pulses generated in the water column and refracted upon entry into the seabed. None of the results could be modeled or explained when the seabed was parameterized as a sand half-space. However, both techniques suggested the presence of a thin muddy layer, 0.05–0.2 m thick within the top 1 m of the sediment. For the arrival angle technique, the layer explains the complicated frequency- and geometry-dependent results; unfortunately, the interference from the layer dominated the arrival angle behavior to the extent that sound speed dispersion could not be unambiguously determined. For the time-of-flight technique, the acoustic wave speed was found to be dispersive in the frequency regime from 0.6 to 20 kHz, with the normalized wave speed increasing from approximately 1.05 to 1.13. However, the buried layer caused the measured sound-speeds to be lower than what a simplified poro-elastic model would predict, unless one accounts for the higher porosity material present within the layer.

Significance: A frequency-dependent sound-speed has numerous implications for the science of underwater acoustics and the practical applications that utilize it, in particular those which extrapolate measurements from one frequency band to another (e.g., sound-speed measured on sediment cores and treated as ground truth for naval sonar). The DRDC results will contribute to the ongoing evaluation of the different theories for sound propagation in marine sediments.

Future plans: The project is complete and no further work is planned.

This page intentionally left blank.

Table of contents

List of figures

List of tables

Acknowledgements

The authors would like to thank the team of divers from the Applied Physics Laboratory, University of Washington, Seattle, and the officers and crew of the R/V Seward Johnson for their support. M. O'Connor, J. Scrutton, M. MacKenzie, D. Caldwell, and I. Haya designed and operated the experimental kit. J. Smith provided expert advice regarding diving operations. The NATO Undersea Research Centre provided technical assistance during collaborative experiments.

This page intentionally left blank.

1 Introduction

1.1 Long-Term Goals and Objectives

Sediment sound-speed measurements during SAX99, a U.S. Office of Naval Research Departmental Research Initiative with a field experiment in 1999 in the Gulf of Mexico, suggested that the speed of sound traveling through marine sediments depends on the frequency of the sound, particularly when the seabed is principally composed of sand [1]. A similar observation has been made in other experiments, such as those in the sand north of Elba Island, Italy [2], [3]. A frequency-dependent sound speed (i.e., sound-speed dispersion) has numerous implications for the science of underwater acoustics and the practical applications that utilize it. Sound-speed dispersion measurements are being used as a fundamental metric for evaluating competing theories, some new and some revived, for sound propagation in marine sediments [4]. Using geophysical measurements made at the site [1], the sound-speed dispersion observed during SAX99 is generally consistent with Biot theory [5] whereas the attenuation is not. There are several potential implications of sound-speed dispersion in marine sediments; one example is the potential misapplication of sound-speed measurements that are made on sediment core samples at high frequencies and then used directly in problems of interest at much lower frequencies, such as in naval sonar.

Historically, it has been difficult to make sound-speed measurements below 10 kHz. As a result, there is a paucity of experimental results and they tend to have large uncertainties, or they are relative rather than absolute values. Measurements in the 1–10 kHz frequency band are critical as this is where the most pronounced sound-speed dispersion was observed during SAX99, and where the most significant differences in model behaviors are predicted to occur [1], [4]. To address these issues, experimental techniques and equipment were developed to measure sound-speed dispersion from approximately 0.1 to 20 kHz during SAX04 [6].

1.2 Approach

1.2.1 Experimental Geometry

The experiment was conducted jointly by the Defence Research & Development Canada – Atlantic (DRDC Atlantic) and The Pennsylvania State University: Applied Research Laboratories (ARL:PSU) in the Gulf of Mexico at 086º38.706'W, 30º23.232'N about 1 km off the coast near Fort Walton Beach, FL, as part of a larger experimental initiative known as SAX04. All measurements were controlled from a portable lab situated aboard the R/V SEWARD JOHNSON, moored due east of the experimental site at a range of 80 m to the closest point on the vessel—the stern. The water depth at the experimental site was approximately 16.7 m. A specially built burial jig was used to deploy six transducers (two projectors and four vector sensors) in the top 1 m of seabed with known horizontal separations. (The vertical position of the transducers and the orientation of the vector sensors were subsequently determined by an optimization technique [6].) After inserting the transducers, the insertion tools and burial jig were removed leaving only the thin electrical leads for each sensor. Fig. 1 is a schematic diagram of the experimental geometry and includes the coordinate system.

The two projectors buried in the seabed, TX_A and TX_D, were ITC-1032 spherical projectors measuring approximately 7 cm in diameter. The in-water source, TX_{ABC}, was a Sensor Technologies SX-100, a cylindrically shaped flextensional projector approximately 6 cm in diameter and 14.8 cm in length. A three-point mooring kept the source at a stable location in the water column and ensured that the seabed directly beneath it was free of any mooring apparatus. The mooring also allowed the grazing angle to be varied from vertical incidence to approximately 25º, while keeping the broad main lobe radiating from the ends of the projector pointing at a reference point on the seabed [6]. Assuming that the properties of the seabed are the same as those from SAX99 [1], as modeled using William's effective density fluid model (EDFM[1]) [7], the critical angle would range from 23.4º to 27.8º in the frequency band from 600 to 3000 Hz.

The buried receivers, denoted *V*1–*V*4, were Wilcoxon model TV-001 "vector sensors," each measuring approximately 4 cm in diameter and 7 cm in length. A vector sensor consists of an all-in-one pressure sensor plus triaxial accelerometer. This combination of signals permits several forms of analysis using: 1) the pressure alone; 2) the acceleration components alone; and 3) combinations of pressure and acceleration signals to calculate acoustic intensity and impedance. When discussing the vector sensors, the subscripts p, x, y, and z will be used to refer to the pressure, and the acceleration in the x-, y-, and z- directions, respectively; e.g., $V1_p$ is the pressure measured by vector sensor *V*1.

1.2.2 Experimental Concepts

Given the single opportunity to make the measurements, and with several unknown factors such as the low-frequency noise levels radiated by the tending vessel, the experimental geometry was designed to enable complementary measurement approaches.

- The grazing angle of sound from an acoustic projector in the water column was varied and the angle of refraction (AOR) into the seabed measured using buried vector sensors at discrete frequencies from 0.6 to 3 kHz. The angle of refraction can be related to the sound speed of the seabed, provided that certain assumptions hold. For these experiments, TX_{ABC} was rotated to ten different positions to create grazing angles from well above to near the nominal critical angle of refraction. Full results of this approach are available in [6] and summarized in this final report. An attempt was also made to extend the low frequency range of the AOR measurements by using the broadband noise radiated by the moored R/V SEWARD JOHNSON as the source of the sound received by the buried vector sensors. Preliminary results are published in [8] but the approach was not pursued any further because of difficulties encountered in correcting for the multipath arrival structure of the ship-radiated noise.
- The time-of-flight (TOF) measurements along all three Cartesian axes were used to measure sound speed in the seabed in the vertical and horizontal directions at discrete frequencies from 0.6 to 20 kHz. The horizontal TOF measurements between buried sources and receivers yielded absolute sound speed dispersion estimates, whereas the vertical TOF measurements were limited to relative estimates due to uncertainty in the depths of the receivers. Full results of this approach are available in [9] and summarized in this final report.

[1] The EDFM is a simplified form of the Biot model that can be derived by setting both the bulk and shear moduli of the sediment frame to zero—a reasonable approximation for sand sediments [1].

- The acoustic impedance of reflected and transmitted arrivals was measured using vector sensors in the water column and buried in the seabed, with the expectation that the amplitude and phase of the impedance of the seabed would depend on the physical properties of the seabed, including sound speed. The acoustic source was positioned directly above two vector sensors buried in the seabed, *V*1 and *V*2 (at depths of 0.61 and 0.98 m below the seabed respectively), and above two vector sensors in the water column, *V*5 and *V*6 (suspended 0.25 and 0.1 m above the seabed respectively). The data appear to be of good quality and are being analyzed as part of a graduate student research project [10]. The analysis completed by DRDC and reported herein focused on the approaches (TOF and AOR) that yield direct measurements of sediment sound speed.
- The reflection loss from the seabed was measured on two omnidirectional receivers in the water column *H*3 and *H*4. However, the fixed experimental geometry meant that only a single experimental realization was available, whereas modeling suggested that an ensemble average would be required at frequencies of 2 kHz and above to distinguish reflection loss from scattering. The lower frequencies, at which a single realization is acceptable, required the use of longer pulses that led to interference between the direct and seabed reflected arrivals. Due to these limitations, this approach was abandoned.

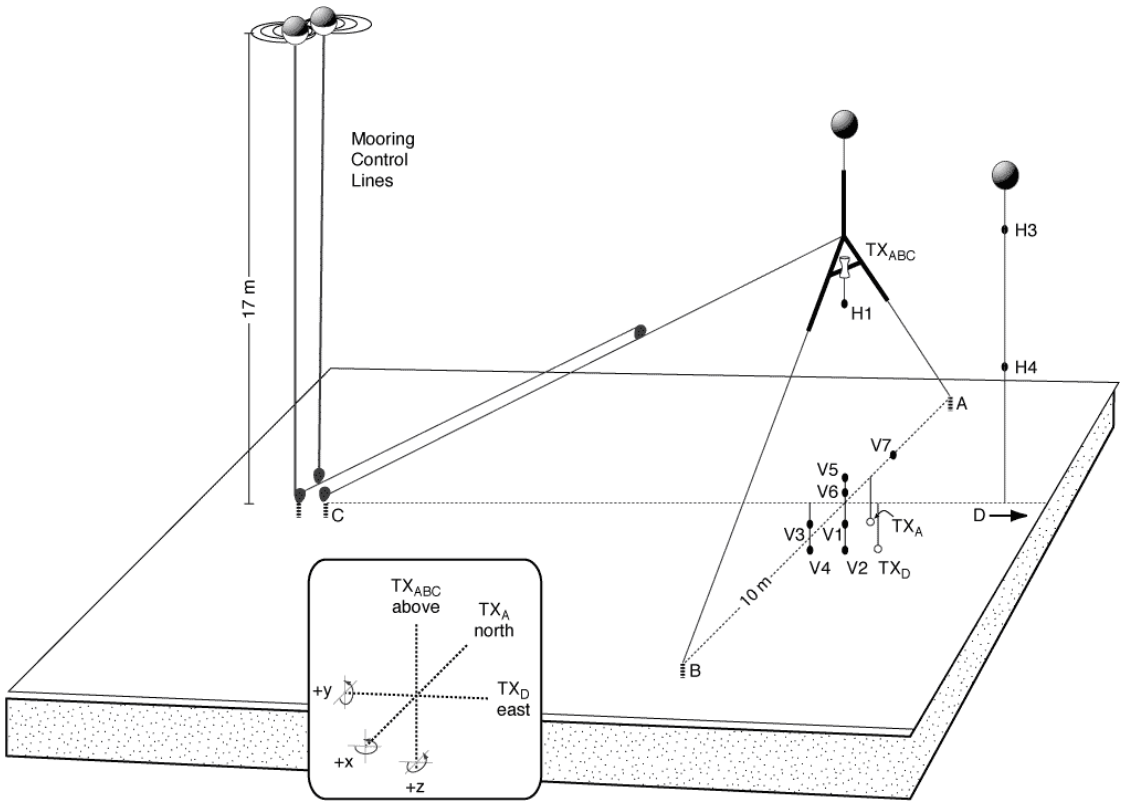

Figure 1: The experimental geometry to measure sound speed dispersion. There are acoustic sources buried in the seabed and in the water column, with a three point mooring to adjust the grazing angle.

2 Work Completed

2.1 Angle of Refraction Technique

2.1.1 Sensor Calibrations

Before the experiment, each vector sensor was calibrated in water at the discrete frequencies used in the experiment. Following the experiment, the calibrations were repeated at several frequencies to confirm that sensors were not damaged during insertion or recovery. The calibrations revealed that the idealized dipole beampattern of the accelerometers is observed on all vector sensors up to at least 4 kHz, hence an ideal dipole response was assumed in the analysis. The amplitude of the acceleration and the pressure time series channels were weighted by their respective sensitivities as calibrated at the center frequency of the pulse being analyzed.

The *z* accelerometer channel on this batch of vector sensors had an unanticipated resonance at 4 kHz. As this channel is used to measure the arrival angles in the *z*-*y* plane (Fig. 1), this effectively limited the AOR approach to 3 kHz and below. The lower frequency limit for all of the experiments involving active transmissions was dictated by the source level of the projectors and ambient noise levels, 0.6 kHz for TX_{ABC} and 0.8 kHz for TX_A and TX_D. The resonance on the *z* accelerometer channel is not related to a soil–sensor coupling interaction as the vector sensors were calibrated in water.

However, this does raise the significant question as to whether the calibrations in water are applicable to sensors buried in the seabed and hence whether "soil–sensor" interaction is a concern. The physics of soil–sensor interaction is considered in detail in [6]. The essential findings are that, for a sensor with the physical attributes of the Wilcoxon model TV-001 vector sensors and a seabed with the properties observed during SAX99 [1], the resonance of the soil–sensor interaction lies within the measurement band from 0.6 to 3 kHz. Crucially, however, the direction of motion of the vector sensor in response to an acoustic wave would remain unaffected as all components of the vector sensor would be affected equally by the soil–sensor interaction. Measurements that only require the relative components along the vector sensor axes to measure arrival angle are likewise unaffected. However, measurements that require the calibrated amplitude of the motion, or combine the accelerometer and pressure channels to calculate acoustic intensity or impedance, must account for the soil–sensor interaction.

2.1.2 Sensor Orientations and Burial Depth

The burial jig designed to release the vector sensors in the seabed [6] was able to constrain their horizontal position to within ±0.01 m. However, there was less control on the vertical placement of the vector sensors as they could be dragged upwards during their release. Preliminary analysis of the vertical TOF data (Section 2.2.2.2) suggested that *V*1–*V*4 did not end up at their intended deployment depth. Further, it became evident—from examining the hodographs of particle motion—that the sensor axes were not aligned with the *x*-, *y*-, and *z*-axes of the experimental geometry [6]. Specifically, the particle motion resulting from transmissions from buried sources TX_A and TX_D and overhead source TX_{ABC} did not align with the known directions of these sources because the orientation of each sensor had become rotated slightly by the deployment

procedure. An optimization technique was devised to reorient and locate the sensors electronically, using signals from sources in the known directions. The technique and resulting sensor depths, rotation axis directions and rotation angles are reported in [6]. The "fit uncertainty" was calculated for each vector sensor as part of the optimization technique. These uncertainties are incorporated into the error bars for the AOR measurements, and also applied in a multi-sensor analysis of seabed properties (Section 2.1.3.4).

The error bars also include the uncertainty associated with the repeatability of the measurements. When the signal-to-noise ratio of the measurement is high, this uncertainty is generally quite small. At the lowest frequencies employed in this experiment, the source level was limited by the capabilities of the projectors and signal-to-noise ratio was a factor, especially for the buried ITC-1032 spherical sources, TX_A and TX_D. The two uncertainties are combined with the assumption that they are uncorrelated.

2.1.3 Measurements and Modelling

2.1.3.1 Observations

The arrival angle in a given plane was determined using the orientation of the major axis of the elliptical particle motion as measured by a pair of acceleration signals [6]. An example is shown in Fig. 2, for sensor *V*4 at source elevation 6 (Table 2 in [6]), at a nominal grazing angle of 42.1º–42.7º assuming that the properties of the seabed accord with the (EDFM) fit [7] to the SAX99 sound-speed measurements [1]. The measured arrival angles show considerable variability as a function of frequency, for this example and for all four vector sensors and all ten grazing angles. They do not exhibit the behaviour anticipated for an isospeed seabed assuming Snell's law of refraction—a constant angle of refraction, nor do they exhibit the behaviour anticipated for a homogenous seabed with a sound-speed dispersion—a relatively gradual and systematic change in arrival angle as a function of frequency (Fig. 2). The pursuit of an explanation for the unexpected behaviour in arrival became a major undertaking in which all assumptions regarding the physics of the sound propagation and the parameterization of the seabed were reconsidered and evaluated.

2.1.3.2 Half-space Seabed Parameterizations

Although ray theory provides an intuitive visualization of acoustic propagation from source to receiver, it has limitations. Rays only coincide exactly with the direction of particle motion and energy flow in specific cases (plane waves, spherical waves). To restore the "diffracted" components of the field (largely made up of the vertically evanescent waves), and to correctly determine particle motion and acoustic intensity, the full wave-theory solution to the acoustic wave equation is required, in general. In fact, the SAX04 experimental conditions do not entirely support the ray theory approximation. In some cases (low frequency, shallow receiver, low grazing angle), the diffracted field becomes important, in which case the particle paths are not longitudinal in the ray direction but elliptical, owing to phase differences between the vertical and horizontal components of particle motion. Moreover, the semi-major ellipse axis may not align with the ray path, in which case analysis using Snell's law would provide erroneous dispersion results. In addition, the arrival angle does not necessarily change monotonically, and it is this characteristic that was initially thought to be responsible for the behavior of the measured arrival

angles. However, the modeled variations (Fig. 2) are far smaller than those observed. The calculations were repeated for different half-space environments but the interaction of the refracted and diffracted fields simply cannot explain the observed behavior in arrival angles.

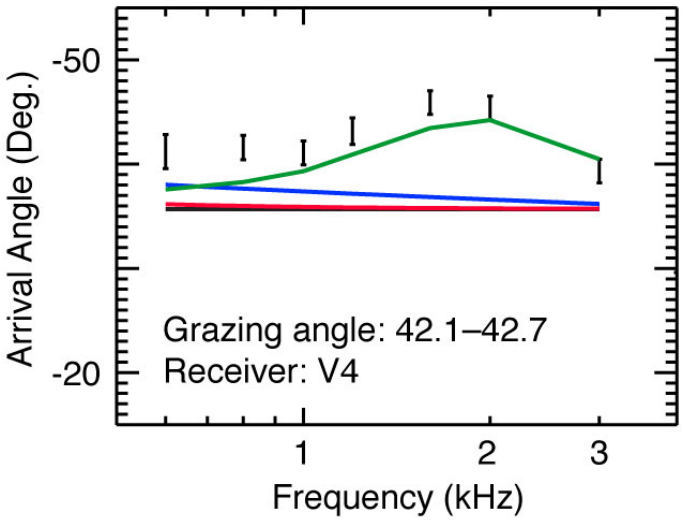

Figure 2: Arrival angles versus frequency measured by buried vector sensor V4 in the z-y plane. The lines represent different model predictions: black, Snell's law of refraction for an isospeed sand half-space; red, the same sand half-space but including the diffracted field; blue, a homogeneous seabed with sound-speed dispersion; green, a thin low-impedance shallow-layer in between isospeed sand layers.

2.1.3.3 Alternate Seabed Paramaterizations

Given the results of the half-space parameterizations (Section 2.1.3.2), it was decided to consider more complex stratified media. This required the OASES model [11], a general-purpose computer code for modeling seismoacoustic propagation in horizontally stratified waveguides, including multiple layers and shear waves if desired, and execution in pulse mode, OASP. OASES was used to evaluate whether one of several alternate parameterizations of the seabed could explain the observed arrival angle behaviour. The following parameterizations were considered but the effects were inadequate to explain the variability in the observed arrival angles.

- Sediment rigidity, by introducing a shear speed of 150 m/s.
- Reflection from a layer of higher impedance at a depth of 3.43 m [12], with and without shear waves.
- A multiple-stacked-layer model based on a power-law compressional wave sound speed of $c_p = c_o(z/z_o)^{0.015}$ where $c_o = 1650$ m/s and $z_o = 1$ m, with and without a power-law shear speed profile of $c_s = c_o(z/z_o)^{0.253}$ where $c_o = 121.5$ m/s and $z_o = 1$ m.

2.1.3.4 Thin Low-Impedance Shallow Layer

To explore the potential influence of a low-impedance layer, OASP model runs were repeated for all combinations of a layer varying in its depth of burial, from 0.1 to 1.3 m with a step size of 0.1 m, and with different thicknesses of 0.01, 0.03, 0.05, 0.1, 0.15, 0.2, and 0.25 m. The properties of the low-impedance layer were assumed to be those of a typical continental shelf environment "clayey-silt" [13, Table IB], but simply referred to as "mud", with a compressional sound speed of 1546 m/s, a density of 1490 kg/m^3, and an attenuation of 0.33 dB/wavelength. (For the variations in arrival angle under consideration, the modeling is insensitive to the attenuation.) The sand above the mud layer, as well as the sand half-space below the mud layer, had the following properties: a compressional sound speed of 1704 m/s, an attenuation of 1.56 dB/wavelength, and a density of 2040 kg/m^3. The sound speed and attenuation for the sand were selected from the value of the EDFM fit to the SAX99 sound-speed measurements at 1.6 kHz, a frequency approximately midway within the AOR measurement band and at which there were measurements during SAX99 [1].

A cost function was defined (root mean square difference in arrival angle) to evaluate the fit of the various model runs to the experimentally measured arrival angles for the "grid" of seabed parameterizations. The cost function was also calculated for a sand half-space model without the mud layer and yielded a value of 4.6º. This value serves as a baseline to quantify the improvement, or degradation that results from the introduction of a low-impedance layer. The contour plot of the cost function for the grid of mud layer burial depth and thickness revealed a minimum of 3.0º for a layer buried at a depth of 1.0 m with a thickness of 0.1 m. The minimum lies in a trough, indicating that good solutions may also be obtained for a thicker layer that is shallower, that is a 0.15 m thick layer buried at 0.95 m or a 0.2 m thick layer buried at 0.9 m.

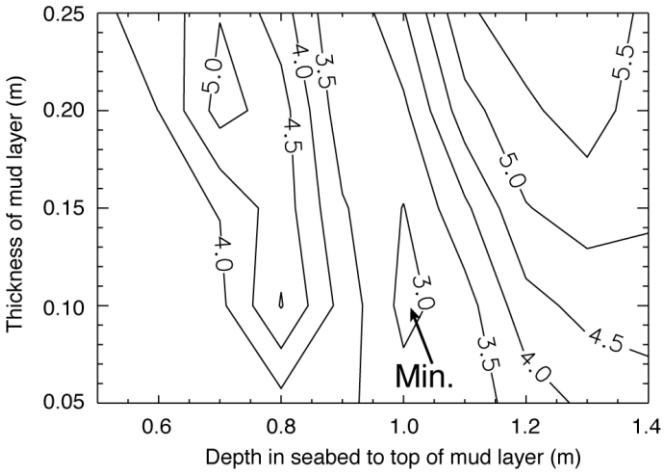

Figure 3: Contour plot of the cost function quantifying the difference between measured and modeled arrival angles for different combinations of the thickness and depth to the top of a mud layer buried within a sand seabed. The location of the cost function minimum is marked by the arrow and labeled "Min.".

To search for seabed properties that reduce the minimum value for the cost function (Fig. 3), the burial depth and thickness of the mud layer were fixed at 1.0 m and 0.1 m, respectively, and

model runs were conducted for different combinations of the mud and sand sound speeds and densities. For the sand and mud, this resulted in compressional sound speeds of 1680 m/s and 1583 m/s, and densities of 2040 kg/m^3 and 1680 kg/m^3, respectively. The grid search of mud layer burial depth and thickness was then repeated to confirm that the position of the cost function minimum had not shifted when using the revised geoacoustic properties. The minimum was found to have remained in the same location with a value of 2.8º.

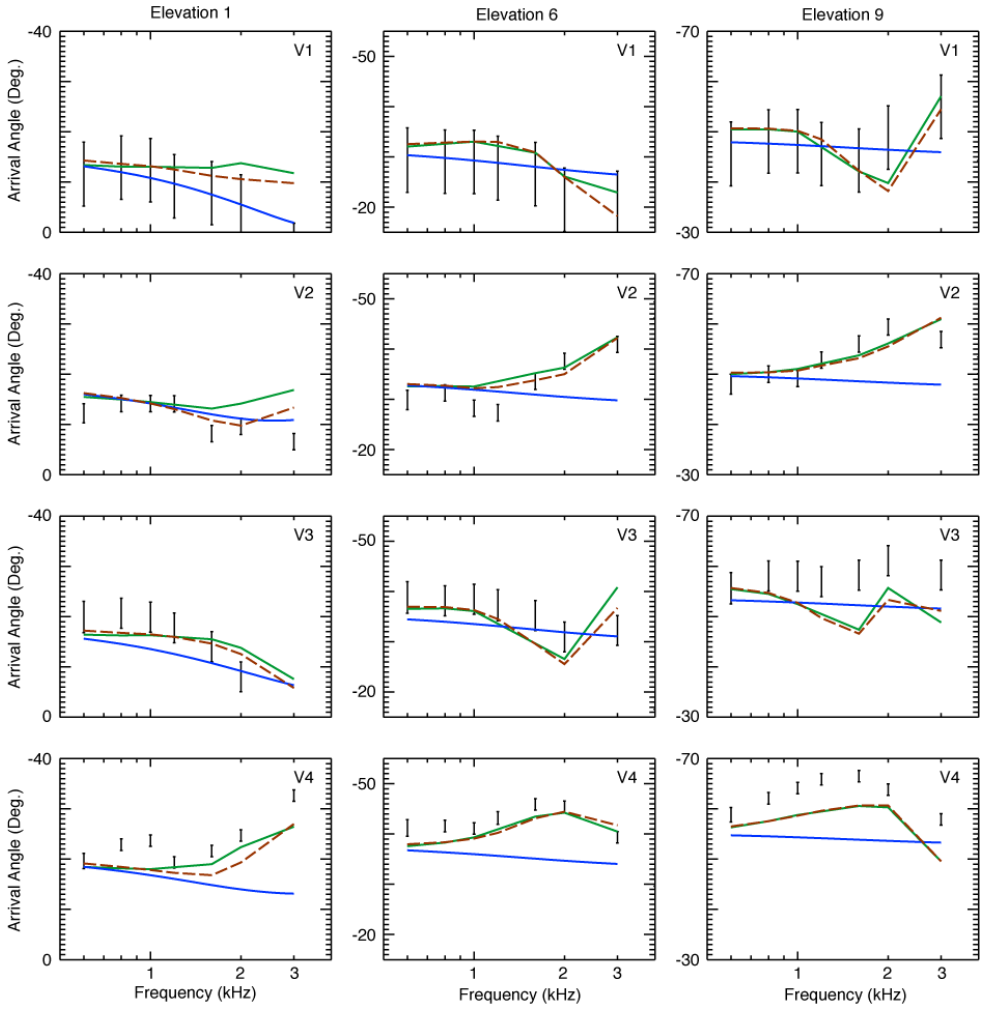

Figure 4: Arrival angles versus frequency measured by the buried vector sensors in the z-y plane. From top to bottom, each row presents a different vector sensor. From left to right, the columns present results for source elevations 1, 6, and 9 (representative of grazing angles slightly-, moderately-, and well-above the nominal critical angle). The lines represent different model predictions: blue, a homogeneous seabed with sound-speed dispersion (same as in Fig. 2); green, the thin low-impedance shallow-layer in between sand layers; brown dashed, same as green but including sound-speed dispersion for the sand layers.

The predicted arrival angles, using the final sand and mud geoacoustic properties and the burial depth and thickness of the mud layer thickness associated with the cost function minimum

(Fig. 3), are plotted in Fig. 4, along with the measured arrival angles. The modeled arrival angles vary considerably depending on the source elevation, receiver location, and frequency. In general, they replicate the complicated behavior observed in the measured data suggesting that a thin low-impedance layer, buried at a depth similar to that of sensors *V*2 and *V*4 (Table 3 in [6]), is a parameterization of the seabed that is capable of explaining the remarkably variable and unexpected arrival angle behavior of the vector sensors.

2.1.4 Discussion

Thus far, the modeling of the buried low-impedance layer has been undertaken with the sand layers having a constant sound speed that is independent of frequency. Given that the objective of the experiment was to measure sound speed dispersion in sand, additional modeling was undertaken to determine if dispersion could be discerned despite the interference from the buried layer. Once again, the burial depth and thickness of the mud layer were fixed at 1.0 m and 0.1 m, respectively. The properties of the mud layer remained the same, with a compressional sound speed of 1583 m/s and a density of 1680 kg/m^3. The properties of the sand layers were set according to the EDFM [7] fit to the SAX99 sound speed measurements [1] at the discrete frequencies used in the experiment.

The arrival angles resulting from this modelling are plotted as the dashed brown lines in Fig. 4. They tend to behave similarly to the isospeed sand case (solid green lines), and the minimum of the cost function remained in the same location with a value of 2.9º (i.e., no improvement). For reference, the sand half-space modelling with sound speed dispersion (Section 2.1.3.2) is repeated in Fig. 4 (solid blue lines).

The arrival angle variations appear to be dominated by the interference effects associated with the thin buried low-impedance layer, with the improvement in the model-data comparison providing support for the presence of the layer. In comparison, the effects of sound speed dispersion in the sand layers are minor. Consequently, it was not possible to pursue the analysis of the arrival angle data to the point of estimating sound speed dispersion in the sand. However, the analysis and modeling of the acceleration signals with the AOR data provided substantial insights regarding the propagation within and nature of the seabed. Without these insights, it is likely that the effects of the buried low-impedance layer on the pressure signals used in the TOF analysis (Section 2.2) would not have been revealed.

2.2 Time of Flight Technique

2.2.1 Data collection and Processing

The buried sources used in the experiment, TX_A and TX_D, and the in-water source, TX_{ABC}, are described in Section 1.2.1. The three point mooring was adjusted such that TX_{ABC} was positioned directly above sensors *V*1 and *V*2, with the broad main lobe from the projector radiating from vertically downward. Along this axis, approximately 1 m from the source, an unamplified omnidirectional hydrophone was positioned (*H*1 in Fig. 1); it served the dual purpose of monitoring the source level of TX_{ABC} and acquiring a replica signal for the data processing.

The pressure sensor in the vector sensor is operational up to frequencies in excess of 40 kHz but the anti-aliasing filter in the data acquisition system limited the upper frequency to 20 kHz. The lower frequency limit was set by the projector bandwidth, 0.6 kHz for the SX-100 (TX_{ABC}) and 1 kHz for the ITC 1032 (TX_A and TX_D). Accordingly, the experiment was performed at frequencies from 600 Hz to 20 kHz. A pulse duration of 5 ms was used for all frequencies for TX_{ABC} so as to maintain a nominal frequency resolution of 200 Hz for the experiment. For the buried projectors, TX_A and TX_D, a 5-ms pulse would have resulted in interference of the interface reflection with the direct arrival and significantly corrupted the TOF estimates (Fig. 5). Therefore, the pulse length employed was based on a compromise at each pulse centre frequency that attempted to minimize multipath interference while maximizing frequency resolution.

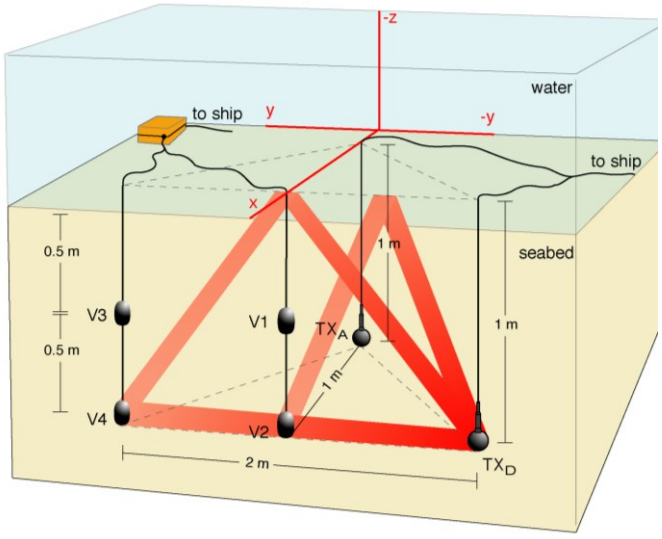

Figure 5: Schematic of the experimental geometry for the TOF experiment. The direct and interface-reflected paths for transmitter TX_D are depicted by the shaded areas. The in-water projector and monitor hydrophone (not shown) were located directly above V1 and V2.

For each frequency of the experiment, a wave train of 50 Hamming weighted pulses was generated. The time series waveform output by the waveform generator, the transmitting voltage and current time series, and the pulse train received by sensors *H*1 and *V*1–*V*4 were all recorded and synchronized to a common time base. Two methods were used to estimate the TOF from which the acoustic wave speed was estimated. The first was the time delay between the first peak on two channels ('peak' in Fig. 6) and the second was by means of replica correlation ('replica' in Fig. 6), whereby a replica of the transmitted pulse was cross correlated with the received signals and the TOF calculated using the correlated time series. To ensure that the replica correlation method did not introduce any additional errors, it was tested by estimating the speed of sound in water (known independently from a conductivity–temperature–depth probe measurement [9]) using transmissions from TX_{ABC}, the monitor hydrophone *H*1 and another hydrophone in the water column (*H*4 in Fig. 1).

2.2.2 Measurements and Modelling

2.2.2.1 Acoustic Wave Dispersion Along Horizontal Axes

With four receivers and three projectors available, there is a plethora of sensor combinations that could be used to obtain horizontal TOF estimates. However, experimental and geometrical restrictions [9] reduced this number considerably such that the primary data employed to obtain sound-speed dispersion from the TOF experiment were paths TX_A–$V2$, TX_D–$V2$, and $V2$–$V4$ using source TX_D (Fig. 6). (The dispersion results are normalized by the wave speed in the overlying water column during the experiment, 1534.3 m/s, to simplify comparison with the results obtained during SAX99.)

The data from path $V2$–$V4$ show a slight bias to higher sound-speed ratios than the results obtained from paths $TX_{A,D}$–$V2$. (Placement errors of the sensors would bias the entire data set from a pair of sensors to higher or lower sound speeds depending on whether the actual path length was shorter or longer than the assumed path length.) In spite of the large spread in the data, a clear frequency dependence emerges in the horizontal plane. The solid line in Fig. 6 is an empirical fit to the data given by $c_s/c_w = 1.07 + 0.04 \cdot \log_{10}(f_{kHz})$ where f_{kHz} is the frequency in kHz.

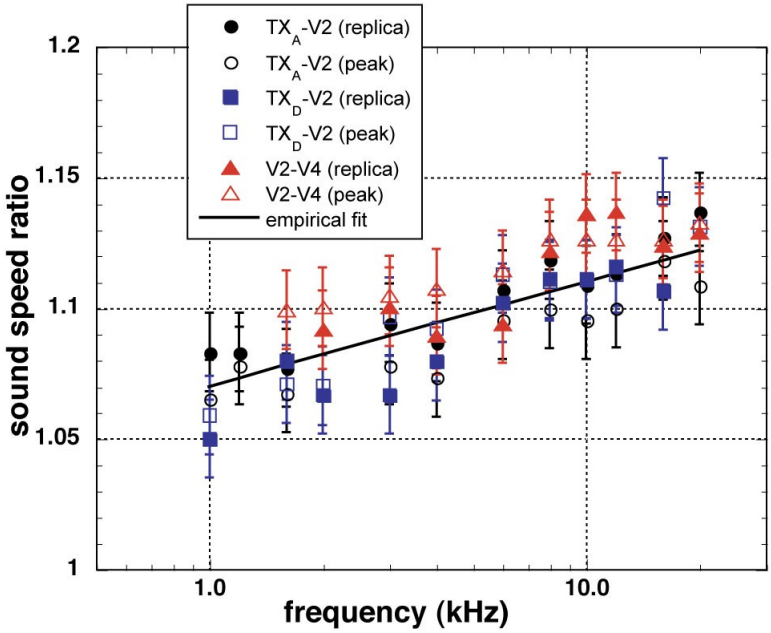

Figure 6: Sound-speed results for three horizontal paths (symbol shapes and colors) and two processing methods (open or filled symbols). The solid line is an empirical fit described in the text. The error bars result from the uncertainty in sensor location.

2.2.2.2 Acoustic Wave Dispersion Along the Vertical Axis

The vertical TOF measurements are shown in Fig. 7a, from $V1$ to $V2$ and from $V3$ to $V4$, both using projector TX_{ABC} as the sound source, and processed with the replica correlation method.

The vertical axis is labelled as "adjusted sound speed ratio" because the accuracy in the depth estimates of sensors *V*1–*V*4 made an absolute measure of the sound speed ratio impractical. The vertical adjustment was chosen to enable comparison with the horizontal dispersion measurement. (The empirical curve from Fig. 6 is plotted again for reference in Fig. 7a.) Data above 6 kHz have been excluded because some anomalous behaviour (attributed to the effect described below) precluded their use in the dispersion analysis. Although the acoustic wave speed shows an increase with frequency, there is an undulation between 1–4 kHz. Furthermore, this undulation is substantially greater for *V*3–*V*4 than for *V*1–*V*2.

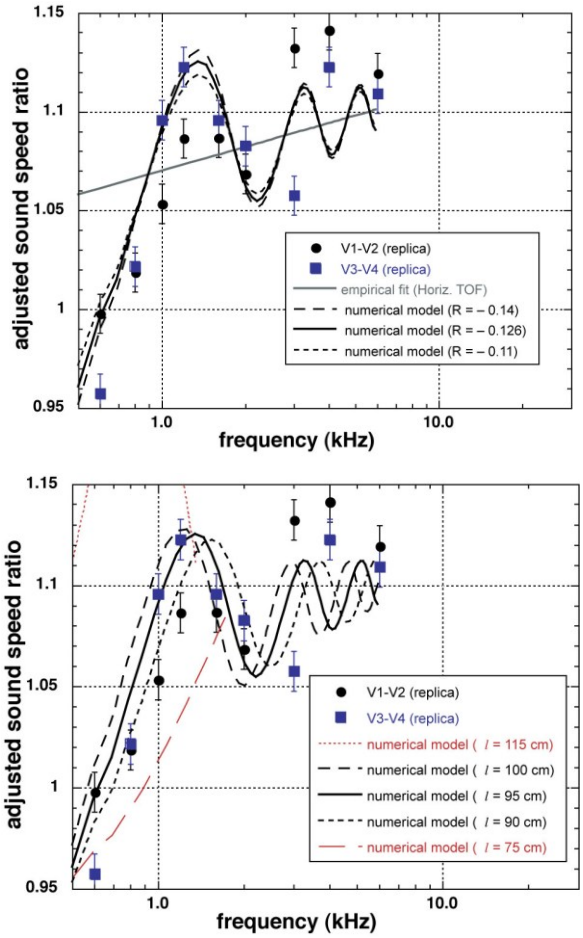

Figure 7: Sound-speed ratio in the sediment for two vertical paths, V1–V2 and V3–V4. The error bars are determined by the temporal resolution of the sampling rate and the error associated with the replica correlation process. The data are compared to results from a numerical model with a low-speed reflecting layer (a) at depth l = 95 cm for three values of reflection coefficient, R, and (b) placed at various depths, l, with R = -0.126.

The undulation in acoustic wave speed is consistent with interference from localized reflectors, such as mud inclusions or thin localized mud layers (mud lenses). This was determined by using a simple numerical model to assess the impact that a reflecting layer (assumed to be infinitesimally thin) would have on the TOF analysis. The pressure time series received at a sensor above the

layer were simulated by coherently summing a direct arrival from TX_{ABC} with a time-delayed version that has been multiplied by pressure reflection coefficient, R. The time-delay is given by $t_d = 2*(l-d_{Vi})/c_s$ where l is the layer depth, d_{Vi} is the depth of sensor Vi, (i = 1, 2, 3, 4), and c_s is the empirical sediment sound speed from Section 2.2.2.1. The apparent TOF is then calculated as a function of frequency using the replica correlation method.

Values of R = -0.126 and l = 95 cm were chosen to visually fit the data from 0.6 to 2 kHz where the data from both sensor pairs have similar trends. As demonstrated in Figs. 7a and 7b, the effects of l and R on the numerical model output are nearly independent of one another; that is to say, l sets the frequency of the maxima and minima whereas R sets their amplitudes. Note that values of l = 90, 95, and 100 cm all provide a reasonable match to the data, whereas the model-data agreement deteriorates completely for l = 75 cm and l = 115 cm. These values of l and R are consistent with the model results from the AOR technique that indicated the presence of a thin, low sound-speed reflecting layer approximately 100 cm deep with R = -0.126 (Section 2.1.3.4).

A simple correction for the multi-path interference can be made to the measured sound speed data using $c_{corr} = c_{meas} + (c_{true} - c_{apparent})$ where c_{corr} is the corrected sound speed data, c_{meas} is the measured sound speed (the data points in Fig. 7), $c_{apparent}$ is the apparent sound speed (the solid line for the model with R = -0.126 and l = 95 cm) that results from the interference, and c_{true} is the "true" sound speed which, for the purpose of correcting for the interference, is presumed to be the empirical curve from the horizontal TOF analysis. The corrected vertical sound speed data from 600 to 2000 Hz are combined with the results obtained for the horizontal estimate in Section 3.1.

2.2.2.3 OASES Pulse Propagation Modelling

For the vertical TOF data, the interference from the low-speed reflecting 'layer' results in a frequency dependence that masks any true sound speed dispersion (Section 2.2.2.2). The layer has a more subtle impact on the horizontal TOF estimates since the arrival of the direct and mud-inclusion-reflected paths are coincident in time within the temporal resolution of the experiment. To investigate the impact on the horizontal TOF, the OASES [11] model was employed. The model was run for a geometry corresponding to source TX_D, and receivers $V2$ and $V4$ (Fig. 5). OASES was used in pulse mode (module OASP) to generate a wave train of 50 Hamming weighted pulses that replicated the experimental procedure. The output generated was the received time series corresponding to the locations of $V2$ and $V4$. Bear in mind that a single, uniform layer is an over-simplification of the environment, and this modeling is only meant only to provide qualitative insight into the results.

OASP was run for several environments: First, a sea-water half-space overlaying a water-saturated sand half-space, separated by a planar boundary at z = 0; second, the same environment modified to include a 10 cm thick mud layer located in the bottom from z = 100 cm to z = 110 cm. A non-dispersive fluid bottom was assumed for both cases. The parameter values used in OASP for compressional wave speed, density, and attenuation for sand and mud are contained in Table 1. These values are typical of sand and mud, are consistent with the modeling results contained in [6], and obtain a reflection coefficient of R = -0.126. One could equally place the top of the layer at a depth of 95 cm based on the results of the vertical TOF modeling (Section 2.2.2.2); however, the exact location of the layer is far less important to the horizontal sound speed dispersion measurements than is its thickness or its depth relative to the buried

sensors. To highlight these effects, two additional scenarios were modeled using OASP. First while maintaining the mud layer at 100–110 cm, receivers *V*2 and *V*4 were placed at 98 cm and 86 cm, respectively which corresponds to the sensor localization estimates computed [6]; finally, the mud layer was increased to 15 cm thickness, from 95–110 cm depth.

Table 1: Parameter inputs used in OASES (OASP) modeling.

Parameter	sand	mud†
wave speed	1680 m/s	1583 m/s
density	2040 kg/m^3	1680 kg/m^3
attenuation	0.84 dB/wavelength	0.33 dB/wavelength

†Mud is a generic term that refers to sand-silt-clay mixtures that are predominantly silt and clay. The term is used in the present context to distinguish it from a purely sand half-space.

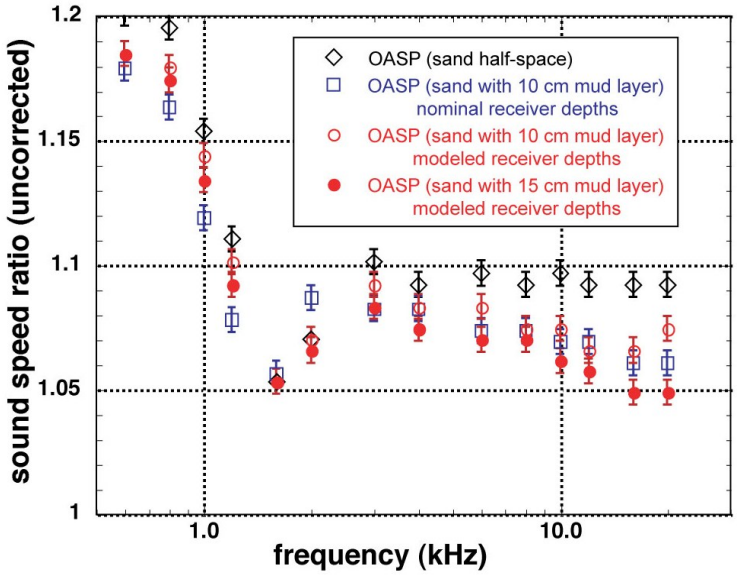

Figure 8: Modeled sound-speed ratio calculated for path V2–V4 from a source located at TX_D, for a sand half-space (open diamonds), and for a sand seabed with a mud layer present from 100 to 110 cm (open squares and open circles) or from 95 to 110 cm (solid circles). The error bars denote the resolution associated with the sampling rate of the time series.

Figure 8 shows the sound speed ratio calculated using the results from the OASP simulation for all four scenarios. The apparent increase in sound speed ratio below 2 kHz for all cases results from the interference of the direct and interface-reflected arrival. Above 2 or 3 kHz, one can time-gate out the interface-reflected arrival and the following comments only pertain to the higher frequencies. The calculated sound speed ratio in the sand half-space is approximately constant with frequency (standard deviation ≈ 0.003) with a mean value of 1.095; this corresponds to the sediment wave speed of 1680 m/s in Table 1. A constant sound speed is expected since dispersion is not included in the model. By contrast, the mud-layer introduces substantially more variability

in the sound speed ratio (standard deviation ≈ 0.01) because of the complicated nature of propagation in this environment; this is in qualitative agreement with the fluctuations in the data in Fig. 6. That is to say, the gentle undulations in the data are more likely due to the presence of a low-sound-speed layer or lens as has been postulated, rather than an intrinsic measurement uncertainty; moreover, different sensor pairs would exhibit slightly different undulations since they would correspond to different displacements from a buried layer if the layer isn't of uniform depth or thickness. This effect is captured in the OASP model by changing the depth of the sensors (open circles and open squares) relative to the simple mud layer used in the model. This is in contrast with the effect of increasing the layer thickness (solid circles)—the undulations are still present of course, but the sound speed ratio is lowered at all frequencies, relative to the results for the 10 cm thick layer. Assuming that 10-15 cm represents the upper limit for the layer thickness, one obtains a mean value of the sound speed ratio for the sand-plus-mud-layer of 1.071 to 1.065; that is, the mud layer lowers the compressional wave speed on average by about 2.4–3%.

2.2.3 Discussion

The OASP model-results showed that the presence of a thin mud layer in a predominantly sand bottom would reduce the sound speed measured with our experimental geometry, and introduce small fluctuations in the sound speed as a function of frequency. The magnitude of and frequencies at which these fluctuations occur will depend on the layer thickness, and the relative depths of the layer, the source, and the receivers. Since the modeled mud layer oversimplifies the experimental conditions, and the depths relative to the layer would be different for different source-receiver pairs, an exact match between the data and the model isn't to be expected; a more reasonable approach would be to average the data obtained along all of the paths at a given frequency to remove some of the frequency fluctuations seen in the data in order to examine the underlying trend. The data from the horizontal and vertical TOF analysis are averaged and plotted in Fig. 9. The vertical bars on the data represent ±1 standard deviation (±1 σ) of the data used in the average.

The dashed line in Fig. 9 is the sound speed estimate for SAX99 using the EDFM [7]. The model was evaluated using the parameters obtained for the SAX99 experiment since the curve is well known to the research community, the measurements were made in similar sediments within a few kilometres of one another, and it provides a comparison of the present data to the SAX99 model results. One might argue that it would be better to use the parameters obtained during SAX04; however, it is entirely possible that the extreme temporal and spatial variability of the seabed that resulted from the passing of Tropical Storm Matthew and Hurricane Ivan through the area could produce results that do not accurately reflect the localized conditions at the DRDC site any better than (or even as well as) those collected during SAX99. (The interested reader is referred to [14] which contains the EDFM model evaluated using the SAX04 parameters.)

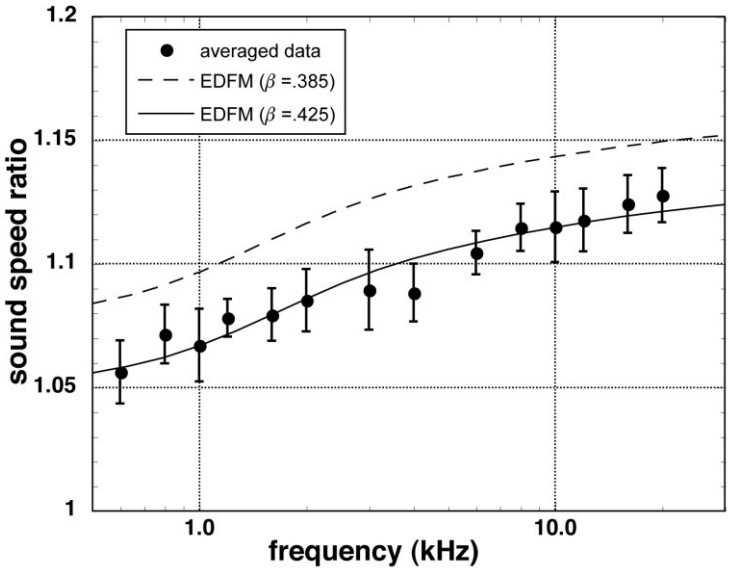

Figure 9: Comparison of the averaged sound-speed ratio versus frequency (sound-speed dispersion) in the sediment obtained along all three coordinate axes (solid circles) to the EDFM (lines) evaluated for two different values of porosity (see text).

There is qualitative agreement in the frequency trend of the data and the EDFM estimate, but the EDFM overestimates the sound speed ratio. However, mud inclusions would act to increase the porosity [15] which would lower the sound speed estimate from the EDFM (See Fig. 1 in [1]). In particular, mud with the parameters shown in Table 1 would have porosity β in the range [15] $0.6 < \beta < 0.7$, so even a thin layer or inclusion would significantly increase the mean value of porosity in the immediate vicinity of the experiment, if a weighted average were computed that included a thin mud layer. To examine the potential impact on the EDFM, the porosity was left as a free parameter to minimize the absolute error between the EDFM and the data. This occurs for $\beta = 0.425$ and is given by the solid curve in Fig. 9. The mean difference in sound speed between the two EDFM estimates is 3%, consistent with the impact of a buried mud layer in the OASP horizontal TOF modeling.

3 Summary

3.1 Results

The DRDC SAX04 sound speed results are overlain on the SAX99 dispersion data reported in [1] in Fig. 10. The acoustic wave speed is dispersive in the frequency regime from 0.6 to 20 kHz with the normalized wave speed increasing from approximately 1.05 to 1.13. Self-consistent results from the OASES modeling of the horizontal TOF, from the simple numerical model developed for the vertical TOF interference pattern, and from the modeling of the complicated arrival angle behaviour observed in the AOR technique, all support the hypothesis that localized mud inclusions are present in the seabed at a depth of approximately 1 m, and could account for the lower sound speed ratio measured at the DRDC site in SAX04 relative to the SAX99 result. This conclusion is supported qualitatively by core samples obtained near the site that show mud inclusions at or near this depth.

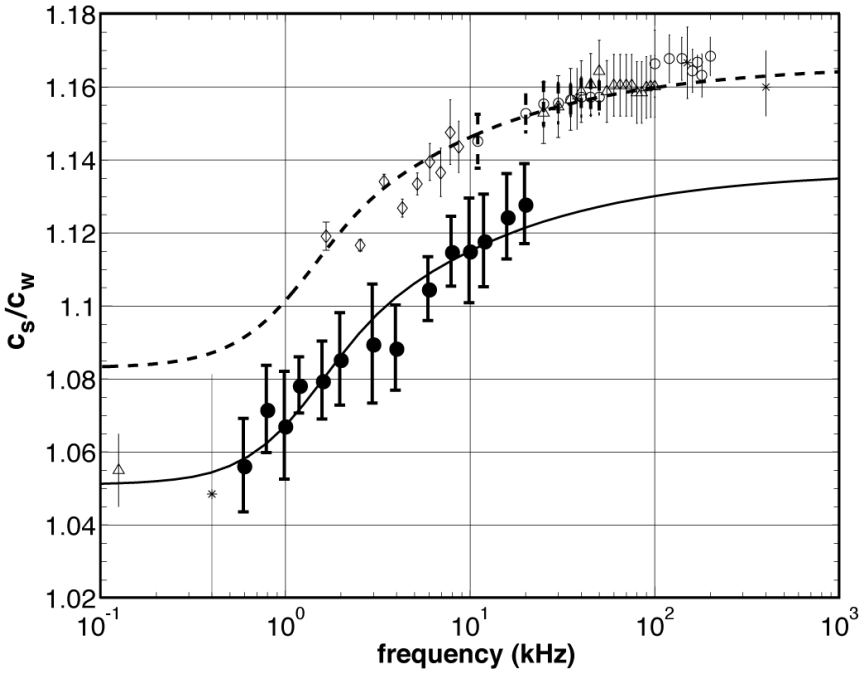

Figure 10: Comparison of the DRDC SAX04 data (solid circles) with the results from SAX99 reported in [1]. The dashed and solid lines are the EDFM model estimates from Fig. 9.

The frequency dependence of the measured sound speed ratios are in good agreement with Williams' [7] poro-elastic model (EDFM) evaluated using physical parameters measured during the SAX99 experiment [1]; however the sound speed ratios for SAX04 are about 3% lower than the EDFM predictions. If the porosity is left as a free parameter in the EDFM, then the model fits the data across the entire frequency band when $\beta = 0.425$. Clearly, the presence of mud would impact other physical parameters in addition to porosity. For example, the permeability and the bulk modulus are lower for unconsolidated mud than for sand [16], [17]; but each of these

parameter changes would also lower the sound speed estimate from the EDFM (see Fig. 1 in [1]) which would simply reduce the porosity increase required to obtain the best fit resulting in $0.385 < \beta < 0.425$. In any case, there is little to be gained by fine-tuning individual parameters since detailed site-specific measurements were not made at the DRDC Atlantic site; but at the very least, it is a reasonable hypothesis that localized mud inclusions would increase the mean porosity and cause the offset between the data and EDFM results.

3.2 Impact/Applications

Several useful tools and techniques were developed that may be of value to other researchers conducting experiments with vector sensors [6]. These include 1) an optimization technique to determine the orientation and burial depth of vector sensors using transmissions from two, or preferably three, quasi-orthogonal directions; 2) using the results of the optimization, the ability to correct the acceleration signals for the rotation of the sensor during its deployment in the seabed and quantify the uncertainty; 3) a method to calculate arrival angle using the acceleration signals by themselves (without the pressure signal) by determining the tilt angle of the semi- major axis of the particle motion; and 4) a capability to model and examine the acoustic field including the well-known geometric acoustics solution (ray theory), the particle motion and factors that can cause it to be elliptical rather than rectilinear, the acoustic intensity and why it may not be aligned with the particle motion, and the contribution from the diffracted (mainly evanescent) field. In addition, by studying the physics of soil–sensor interaction, there were several lessons learned concerning the deployment of buried vector sensors and recommendations for any future experiments of a similar nature (see Appendix I in [6]).

3.3 Transitions

The sound speed measurements reported herein are published in the open literature [9] and available to researchers developing and evaluating models for sound propagation in marine sediment.

3.4 Related Projects

The acoustic impedance data collected by DRDC during SAX04 are being analyzed and modeled by a graduate student, Mr. Steven Crocker at the Naval Undersea Warfare Center, under the supervision of Dr. James Miller at the University of Rhode Island.

References

[1] K. L. Williams, D. R. Jackson, E. I. Thorsos, D. Tang, and S. G. Shock, "Comparison of sound speed and attenuation measured in a sandy sediment to predictions based on the Biot theory of porous media," *IEEE J. Ocean. Eng.*, vol. 27, no. 3, pp. 413–428, 2002.

[2] A. Maguer, W. L. J. Fox, H. Schmidt, E. Pouliquen, and E. Bovio, "Mechanisms for subcritical penetration into a sandy bottom: Experiment and modeling results propagation," *J. Acoust. Soc. Amer.*, vol. 107, no. 3, pp. 1215–1225, 2000.

[3] A. Maguer, E. Bovio, and W. L. J. Fox, "In situ estimation of sediment sound speed and critical angle," *J. Acoust. Soc. Amer.*, vol. 108, no. 3, pp. 987–996, 2000.

[4] M. J. Buckingham, "Wave propagation, stress relaxation, and grain-to-grain shearing in saturated, unconsolidated marine sediments," *J. Acoust. Soc. Amer.*, vol. 108, no. 6, pp. 2796–2815, 2000.

[5] M. A. Biot, "Generalized theory of acoustic propagation in porous dissipative media," *J. Acoust. Soc. Amer.*, vol. 34, no. 5, pp. 1254–1264, 1962.

[6] J. C. Osler, D. M. F. Chapman, P. C. Hines, G. P. Dooley, and A. P. Lyons, "Measurement and modeling of seabed particle motion using buried vector sensors", *IEEE J. Ocean Eng.*, 35, 516–537, 2010.

[7] K. L. Williams, "An effective density fluid model for acoustic propagation in sediments derived from Biot theory," *J. Acoust. Soc. Amer.*, vol. 110, no. 5, pp. 2276–2281, 2001.

[8] A. P. Lyons, J. C. Osler, and P. C. Hines, "Estimating sound speed dispersion using ship noise measurements," *in Proc. Underwater Acoustic Measurements: Technol. Results*, Heraklion, Crete, Greece, pp. 317–324, 2005.

[9] P. C. Hines, J. C. Osler, J. Scrutton, and L. J. S. Halloran, "Time-of-flight measurements of acoustic wave speed in a sandy sediment at 1-20 kiloHertz", *IEEE J. Ocean Eng.*, vol. 35, pp. 502–515, 2010.

[10] S. E. Crocker, J. H. Miller, K. B. Smith, P. C. Hines, and J. C. Osler, "Geoacoustic inversion using specific acoustic impedance," *J. Acoust. Soc. Amer.*, vol. 126, no. 4, pp. 2234, 2009.

[11] H. Schmidt, OASES 2.2, Massachusetts Inst. Technol., Cambridge, MA, 1999 [Online]. Available: http://acoustics.mit.edu/faculty/henrik/ oases/oases.html.

[12] P. C. Hines, J. C. Osler, J. Scrutton, D. M. F. Chapman, and A. P. Lyons, "Using buried vector sensors to examine seabed layering in sandy sediment," *J. Acoust. Soc. Amer.*, vol. 120, no. 5, pp. 3181, 2006.

[13] E. L. Hamilton, "Geoacoustic modeling of the sea floor," *J. Acoust. Soc. Amer.*, vol. 68, no. 5, pp. 1313–1340, 1980.

[14] B. T. Hefner, D. R. Jackson, K. L. Williams, and E. I. Thorsos, "Mid-to high-frequency acoustic penetration and propagation measurements in a Sandy sediment," *IEEE J. Ocean. Eng.*, vol. 34, no. 4, pp. 372–387, 2009.

[15] M. D. Richardson, K. B. Briggs, S. J. Bentley, D. J. Walter, and T. H. Orsi, "Biological and hydrodynamic effects on physical and acoustic properties of sediments off the Eel River, California," *Mar. Geol.*, vol. 182, pp. 121–139, 2002.

[16] E. L. Hamilton, "Elastic properties of marine sediments," *J. Geophys. Res.*, vol. 76, no. 2, pp. 579–604, 1971.

[17] W. C. Vaughan, K. B. Briggs, J.-W. Kim, T. S. Bianchi, and R. W. Smith, "Storm-generated sediment distribution along the northwest Florida inner continental shelf," *IEEE J. Ocean. Eng.*, vol. 34, no. 4, pp. 495–515, 2009.

List of symbols/abbreviations/acronyms/initialisms

AOR	Angle-of-refraction
ARL:PSU	The Pennsylvania State University: Applied Research Laboratories
DRDC	Defence Research and Development Canada
EDFM	Effective density fluid model
OASES	Ocean acoustics and seismic exploration synthesis
OASP	OASES pulse module
SAX04	Sediment acoustics experiment 2004
SAX99	Sediment acoustics experiment 1999
TOF	Time-of-flight

This page intentionally left blank.

DOCUMENT CONTROL DATA

(Security classification of title, body of abstract and indexing annotation must be entered when the overall document is classified)

1. ORIGINATOR (The name and address of the organization preparing the document. Organizations for whom the document was prepared, e.g. Centre sponsoring a contractor's report, or tasking agency, are entered in section 8.)

DRDC Atlantic
PO Box 1012,
Dartmouth, NS, B2YZ7

2. SECURITY CLASSIFICATION (Overall security classification of the document including special warning terms if applicable.)

UNCLASSIFIED
(NON-CONTROLLED GOODS)
DMC A
REVIEW: GCEC JUNE 2010

3. TITLE (The complete document title as indicated on the title page. Its classification should be indicated by the appropriate abbreviation (S, C or U) in parentheses after the title.)

Measurement and Analysis of Sound Speed Dispersion During SAX04: Final Report for Office of Naval Research Award N000140310883

4. AUTHORS (last name, followed by initials – ranks, titles, etc. not to be used)

Osler, J.C.; Hines, P.C.

5. DATE OF PUBLICATION (Month and year of publication of document.)	6a. NO. OF PAGES (Total containing information, including Annexes, Appendices, etc.)	6b. NO. OF REFS (Total cited in document.)
December 2010	36	17

7. DESCRIPTIVE NOTES (The category of the document, e.g. technical report, technical note or memorandum. If appropriate, enter the type of report, e.g. interim, progress, summary, annual or final. Give the inclusive dates when a specific reporting period is covered.)

External Client Report

8. SPONSORING ACTIVITY (The name of the department project office or laboratory sponsoring the research and development – include address.)

US Office of Naval Research
875 N Randolph Street, Suite 1425, Code 321OA,
Arlington, VA 22203-1995, USA

9a. PROJECT OR GRANT NO. (If appropriate, the applicable research and development project or grant number under which the document was written. Please specify whether project or grant.)	9b. CONTRACT NO. (If appropriate, the applicable number under which the document was written.)
N000140310883 Grant	

10a. ORIGINATOR'S DOCUMENT NUMBER (The official document number by which the document is identified by the originating activity. This number must be unique to this document.)	10b. OTHER DOCUMENT NO(s). (Any other numbers which may be assigned this document either by the originator or by the sponsor.)
DRDC Atlantic ECR 2010-338	

11. DOCUMENT AVAILABILITY (Any limitations on further dissemination of the document, other than those imposed by security classification.)

Unlimited

12. DOCUMENT ANNOUNCEMENT (Any limitation to the bibliographic announcement of this document. This will normally correspond to the Document Availability (11). However, where further distribution (beyond the audience specified in (11) is possible, a wider announcement audience may be selected.))

Unlimited

13. ABSTRACT (A brief and factual summary of the document. It may also appear elsewhere in the body of the document itself. It is highly desirable that the abstract of classified documents be unclassified. Each paragraph of the abstract shall begin with an indication of the security classification of the information in the paragraph (unless the document itself is unclassified) represented as (S), (C), (R), or (U). It is not necessary to include here abstracts in both official languages unless the text is bilingual.)

Sharing the same experimental apparatus, two complementary techniques were developed to measure the frequency-dependent speed of sound in marine sediments during the SAX04 sea-trial. The first technique enabled direct time-of-flight measurements of acoustic wave speed along all three Cartesian axes. The second technique determined the acoustic wave speed based on the arrival angle of pulses generated in the water column and refracted upon entry into the seabed. None of the results could be modeled or explained when the seabed was parameterized as a sand half-space. However, both techniques suggested the presence of a thin muddy layer, 0.05–0.2 m thick within the top 1 m of the sediment. For the arrival angle technique, the layer explains the complicated frequency- and geometry-dependent results; unfortunately, the interference from the layer dominated the arrival angle behavior to the extent that sound speed dispersion could not be determined unambiguously. For the time-of-flight technique, the acoustic wave speed was found to be dispersive in the frequency regime from 0.6 to 20 kHz with the normalized wave speed increasing from approximately 1.05 to 1.13. However, the layer caused the measured sound speeds to be lower than what a simplified poro-elastic model would predict, unless one accounts for the higher porosity material present within the buried layer.

14. KEYWORDS, DESCRIPTORS or IDENTIFIERS (Technically meaningful terms or short phrases that characterize a document and could be helpful in cataloguing the document. They should be selected so that no security classification is required. Identifiers, such as equipment model designation, trade name, military project code name, geographic location may also be included. If possible keywords should be selected from a published thesaurus, e.g. Thesaurus of Engineering and Scientific Terms (TEST) and that thesaurus identified. If it is not possible to select indexing terms which are Unclassified, the classification of each should be indicated as with the title.)

Sediment acoustics; sound speed dispersion.

This page intentionally left blank.

Defence R&D Canada

Canada's leader in defence
and National Security
Science and Technology

R & D pour la défense Canada

Chef de file au Canada en matière
de science et de technologie pour
la défense et la sécurité nationale

DEFENCE DÉFENSE

www.drdc-rddc.gc.ca